Analytical Solution of Scattering by a 2D Dielectric Filled Crack in a Ground Plane Coated by a Dielectric Layer: TM Case

B. Ghalamkari [1], A Tavakoli [1, 2], and M. Dehmollaian[3]

[1] Department of Electrical Engineering,
[2] Institute of Communications Technology and Applied Electromagnetics
Amirkabir University of Technology, Tehran, 15914, Iran
B.Ghalamkari@aut.ac.ir, Tavakoli@aut.ac.ir

[3] Department of Electrical and Computer Engineering
University of Tehran, Tehran, 14395-515, Iran
M.Dehmollaian@ece.ut.ac.ir

Abstract **─** In this paper, KP method is applied to study the scattering of a 2D loaded crack on a ground plane, coated by a dielectric layer for TM case. For simplicity, the geometry is divided into three regions, whose fields are expressed in terms of Bessel eigen functions. The governing equations involve several infinite summations with infinite number of unknown coefficients. By the use of Weber-Schafheitlin discontinuous integrals, these infinite summations could efficiently be truncated with high numerical accuracy. Boundary conditions are applied to determine unknown coefficients. We employ finite element method (FEM) and convergence analysis to confirm our results. Finally, the influence of coating dielectric layer and filling material is investigated on the scattered field.

Index Terms **─** 2D coated crack, dielectric layer, Kobayashi and Nomura method, plane wave scattering, and Weber-Schafheitlin discontinuous integrals.

I. INTRODUCTION

An assessment of the surface cracks is a significant area under discussion in nondestructive testing and evaluation (NDT/NDE). There are two main near-field category techniques reported by the engineering community for crack detection. These methods are based on waveguide techniques [1-3] and the resonator method [4-6]. These techniques are not applicable to the non-accessible cracks like those on boilers or blast furnaces, thus, far-field electromagnetic (EM) scattering measurement is recommended.

The scattering from the rectangular crack can be approached in a variety of ways including the method of moment (MoM) [7], quasi-static approach [8, 9], approximate boundary conditions (ABC) [10, 11], Fourier spectrum analysis [12], finite element boundary integral method (FE-BI) [13], transparent boundary condition (TBC) [14], and overlapping T-block method [15-17]. Additionally, Morgan and Schwering utilized mode expansion scattering solution for wide rectangular cracks in 2D [18] and cavities in 3D [19]. Deek et al. extracted the natural frequency poles with matrix pencil method (MPM) for detecting cracks in buried pipes [20]. Bozorgi *et al.* reported a direct integral equation solver (DIES) method for determining the backscattering signatures of a crack in a metallic surface by omitting singularities in hyper singular integrals [21, 22]. Honarbakhsh *et al.* presented mesh free collocation method for 2D filled crack in infinite ground [23].

The Kobayashi potential (KP) is an analytical technique for solving mixed boundary problems and it has been applied to various EM scattering problems [24-32]. KP utilizes the discontinuity properties of Weber-Schafheitlin's integrals and is closely related to MoM approach. Some of the advantages of KP method are cited here. First, the

Submitted On: Aug. 28, 2012
Accepted On: Mar. 30, 2013

KP method is accurate and simple in the sense of not dealing with singularity of the Green's functions. Second, the solution converges rapidly due to the satisfaction of a part of the boundary condition by each basis function involved in the integrand [31].

Hongo *et al.* used KP method to find scattering of EM spherical wave from a PEC disk [24]. Imran *et al.* utilized this method to compute diffraction of plane wave from a perfectly electromagnetic conductor (PEMC) strip [25]. Sato *et al.* used KP method to analyze TM plane wave scattering by a 2D filled rectangular crack on a ground plane without any dielectric coating [26]. They applied KP method to two rectangular troughs on a ground plane [27] with a standard impedance boundary condition (SIBC) [28] and estimated the depth of the crack [29]. They also used KP method to model the propagation through slits array [30].

In most cases, paint, primer, rust, and oil coat the corrosion (crack) and it cannot be visually detected. Near-field techniques for detecting cracks under paint were applied [1, 3] but a fast, accurate and rigorous method for analyzing the scattering signature of the coating crack with far-field methods is in demand. Previously, EM plane wave scattering by a 2D rectangular gap in a PEC ground plane, coated by a dielectric layer was reported for TE case [32]. In this paper, the TM case of this problem is investigated.

The paper is organized as follows. In section II the KP method is used to derive the governing field equations with unknown excitation coefficients and truncated unknown excitation coefficients are computed. The numerical results and validations are shown in section III. Conclusion remarks are provided in section IV. Here, the time harmonic factor $e^{-i\omega t}$ is assumed throughout the context.

II. PROBLEM DISCRIPTION AND FORMULATION

We assume a dielectric rectangular crack that is filled by a dielectric material and is coated by a dielectric slab. The cross section for the crack is $2a \times b$ and the height of the slab is y_t as shown in Fig. 1. The relative permittivity and permeability of the filling material are ε_r and μ_r, respectively, and (ε_1, μ_1) are of the coating material. The filling and the coating materials could be both lossy, meaning that ε_r, μ_r, ε_1, and μ_1 could be complex.

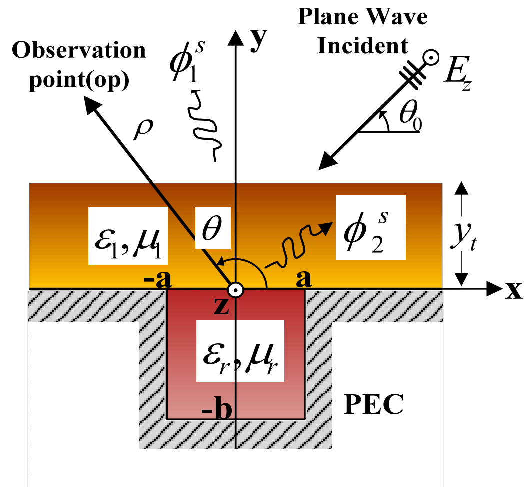

Fig. 1. Geometry of the filled rectangular crack underneath a coating layer in an infinite ground plane.

The incident angle is θ_0 and the observation point is represented by ρ and θ in the cylindrical coordinate system. Assuming ψ is the total electric field in a dielectric slab. The crack is filled by a material with relative permittivity and permeability of ε_r and μ_r, respectively. The relative permittivity and permeability of the slab are ε_1 and μ_1, respectively.

A. Expansion of electromagnetic fields

The geometry of the problem is divided into three regions, which are described as follows.

Region I: Semi-infinite half space $\left(y > y_t\right)$

In this region the total z-component of the electric field is denoted by $\phi_t^1 = E_z$ which is,

$$\phi_1^t = \phi^i + \phi^r + \phi_1^s, \tag{1}$$

where, ϕ^i and ϕ^r represent the incident and the reflected field, respectively. Additionally, ϕ_1^S characterizes the scattering contribution of the crack in this region. The material in this region is free space (ε_0, μ_0).

Region II: Slab Region $\left(y_t > y > 0\right)$

The total z-component of the electric field in this region is given by,

$$\phi_2^t = \psi + \phi_2^s. \tag{2}$$

Here, ψ is the total electric field in the dielectric slab and its calculation is given in the Appendix. Scattering contribution of the crack in this region is denoted by ϕ_2^S.

Region III: Cavity Region $\left(-b \le y < 0, |x| < a\right)$

This region is like a parallel plate waveguide. Therefore, the total field is expressed by a summation of waveguide modal eigenfunctions. Considering the boundary conditions at $x = \pm a$ and $y = -b$, ϕ_3^t is given by,

$$\phi_3^t = \sum_{n=0}^{\infty} L_n \left\{ e^{-ih_n y} - e^{ih_n(y+2b)} \right\} \sin\left(\frac{n\pi}{2}\left(1 - \frac{x}{a}\right)\right) \tag{3}$$

where $h_n = \sqrt{\varepsilon_r \mu_r k_0^2 - (n\pi/w)^2}$ stands for the propagation constant of the n^{th} parallel plate waveguide mode and L_n is the excitation coefficient inside cavity region.

B. Applying KP method for scattering fields

In this section, the scattering fields ϕ_i^s (i = 1, 2) are derived by utilizing the KP method and the boundary conditions are applied to find the unknown coefficients. Since the scattering fields ϕ_i^s (i = 1, 2) satisfy the homogeneous Helmholtz equation, they could be represented as an integral of the general solutions by using the separation of variables method [26]. Without loss of generality, all variables and parameters are normalized with respect to a as follows,

$$u = \frac{x}{a},\quad v = \frac{y}{a},\quad k_0 = \frac{\kappa_0}{a}, k_1 = \frac{\kappa_1}{a}, t = \frac{y_t}{a}, \tag{4}$$

therefore,

$$\phi_1^s = \frac{1}{a}\int_0^{\infty} \left\{ d(\xi/a)\cos(\xi\, u) + e(\xi/a)\sin(\xi\, u) \right\} e^{-v\sqrt{\xi^2-\kappa_0^2}} d\xi \tag{5}$$

and

$$\phi_2^s = \frac{1}{a}\int_0^{\infty} \left\{ f(\xi/a)\cos(\xi\, u) + g(\xi/a)\sin(\xi\, u) \right\} e^{-v\sqrt{\xi^2-\kappa_1^2}} d\xi + \frac{1}{a}\int_0^{\infty} \left\{ h(\xi/a)\cos(\xi\, u) + k(\xi/a)\sin(\xi\, u) \right\} e^{(v-t)\sqrt{\xi^2-\kappa_1^2}} d\xi, \tag{6}$$

where, d(.), e(.), f(.), g(.), h(.), and k(.) denote the unknown weighting functions. It is notable that ϕ_1^s includes only the up-going wave, while ϕ_2^s contains both up-going and down-going waves. Noting the relation between trigonometric and Bessel functions,

$$\begin{cases} \cos(\xi u) = \sqrt{\dfrac{\pi \xi u}{2}} J_{-1/2}(\xi u), \\ \sin(\xi u) = \sqrt{\dfrac{\pi \xi u}{2}} J_{1/2}(\xi u). \end{cases} \tag{7}$$

The weighting functions are expanded in term of the Bessel functions. Thus,

$$\begin{Bmatrix} d \\ f \\ h \end{Bmatrix}(\xi/a) = \sum_{m=0}^{\infty} \begin{Bmatrix} D_m \\ F_m \\ H_m \end{Bmatrix} \frac{J_{2m+1}(\xi)}{\xi} a, \tag{8}$$

and

$$\begin{Bmatrix} e \\ g \\ k \end{Bmatrix}(\xi/a) = \sum_{m=0}^{\infty} \begin{Bmatrix} E_m \\ G_m \\ K_m \end{Bmatrix} \frac{J_{2m+2}(\xi)}{\xi} a. \tag{9}$$

By substituting equations (8) and (9) into equations (5) and (6) we have,

$$\phi_1^s = \sqrt{\frac{\pi u}{2}} \sum_{m=0}^{\infty}\int_0^{\infty} \frac{1}{\sqrt{\xi}} \begin{Bmatrix} D_m J_{2m+1}(\xi) J_{-\frac{1}{2}}(\xi\, u) \\ +E_m J_{2m+2}(\xi) J_{\frac{1}{2}}(\xi\, u) \end{Bmatrix} . e^{-v\sqrt{\xi^2-\kappa_0^2}} d\xi, \tag{10}$$

and

$$\phi_2^s = \sqrt{\frac{\pi u}{2}} \sum_{m=0}^{\infty}\int_0^{\infty} \frac{1}{\sqrt{\xi}} \begin{Bmatrix} F_m J_{2m+1}(\xi) J_{-\frac{1}{2}}(\xi u) \\ +G_m J_{2m+2}(\xi) J_{\frac{1}{2}}(\xi u) \end{Bmatrix} e^{-v\sqrt{\xi^2-\kappa_1^2}} d\xi + \sqrt{\frac{\pi u}{2}} \sum_{m=0}^{\infty}\int_0^{\infty} \frac{1}{\sqrt{\xi}} \begin{Bmatrix} H_m J_{2m+1}(\xi) J_{-\frac{1}{2}}(\xi u) \\ +K_m J_{2m+2}(\xi) J_{\frac{1}{2}}(\xi u) \end{Bmatrix} e^{(v-t)\sqrt{\xi^2-\kappa_1^2}} d\xi. \tag{11}$$

In equations (10) and (11), all integrals are identified as a class of Weber-Schafheitlin integrals, which automatically satisfy the zero tangential electric field boundary condition on a part of the ground plane where $|u| > 1, v = 0$.

C. Boundary conditions

The unknown coefficients of the fields consisting of D_m, E_m, F_m, G_m, H_m, K_m, and L_n are determined by applying the boundary conditions.

The boundary conditions at the interface between regions *I* and *II*, where $v = t\left(y = y_t\right)$, are given by,

$$\begin{cases} \phi_1^s = \phi_2^s & BC.1 \\ \dfrac{\partial}{\partial v}\phi_1^s = \dfrac{\partial}{\mu_1 \partial v}\phi_2^s . & BC.2 \end{cases} \tag{12}$$

Also the boundary conditions at the interface between regions *II* and *III*, where $v = 0\left(y = 0\right)$, are

$$\begin{cases} \phi_2^t = \phi_3^t & BC.3 \\ \dfrac{\partial}{\mu_1 \partial v}\phi_2^t = \dfrac{\partial}{\mu_r \partial v}\phi_3^t . & BC.4 \end{cases} \tag{13}$$

By substituting equations (12) and (13) and equations (7) and (9) into equations (10) and (11) and after some mathematical manipulation, the following equations are derived,

$BC.1$:

$$\begin{aligned} &\sum_{m=0}^{\infty}\int_0^{\infty}\frac{1}{\xi}\left\{ D_m G_{2m+1}^C(\xi) + E_m G_{2m+2}^S(\xi)\right\} e^{-t\sqrt{\xi^2-\kappa_0^2}}d\xi \\ &=\sum_{m=0}^{\infty}\int_0^{\infty}\frac{1}{\xi}\left\{ F_m G_{2m+1}^C(\xi) + G_m G_{2m+2}^S(\xi)\right\} e^{-t\sqrt{\xi^2-\kappa_1^2}}d\xi \\ &+\sum_{m=0}^{\infty}\int_0^{\infty}\frac{1}{\xi}\left\{ H_m G_{2m+1}^C(\xi) + K_m G_{2m+2}^S(\xi)\right\} d\xi \end{aligned} , \tag{14}$$

$BC.2$:

$$\begin{aligned} &\mu_1\sum_{m=0}^{\infty}\int_0^{\infty}\frac{\sqrt{\xi^2-\kappa_0^2}}{\xi}\left\{ D_m G_{2m+1}^C(\xi) + E_m G_{2m+2}^S(\xi)\right\} e^{-t\sqrt{\xi^2-\kappa_0^2}}d\xi \\ &=\sum_{m=0}^{\infty}\int_0^{\infty}\frac{\sqrt{\xi^2-\kappa_1^2}}{\xi}\left\{ F_m G_{2m+1}^C(\xi) + G_m G_{2m+2}^S(\xi)\right\} e^{-t\sqrt{\xi^2-\kappa_1^2}}d\xi \\ &-\sum_{m=0}^{\infty}\int_0^{\infty}\frac{\sqrt{\xi^2-\kappa_1^2}}{\xi}\left\{ H_m G_{2m+1}^C(\xi) + K_m G_{2m+2}^S(\xi)\right\} d\xi \end{aligned} , \tag{15}$$

$BC.3$:

$$\begin{aligned} &\sum_{k=0}^{\infty}(-1)^k\left\{\begin{array}{l} L_{2k+1}\gamma_{2k+1}\cos\left(\dfrac{2k+1}{2}\pi u\right) \\ +L_{2k+2}\gamma_{2k+2}\sin\left((k+1)\pi u\right)\end{array}\right\} = \\ &\sum_{m=0}^{\infty}\int_0^{\infty}\frac{1}{\xi}\left\{ F_m G_{2m+1}^C(\xi) + G_m G_{2m+2}^S(\xi)\right\} d\xi \\ &+\sum_{m=0}^{\infty}\int_0^{\infty}\frac{1}{\xi}\left\{ H_m G_{2m+1}^C(\xi) + K_m G_{2m+2}^S(\xi)\right\} e^{-t\sqrt{\xi^2-\kappa_1^2}}d\xi \end{aligned} , \tag{16}$$

$BC.4$:

$$\begin{aligned} &-\frac{\mu_1}{\mu_r}\sum_{k=0}^{\infty}(-1)^k\left\{\begin{array}{l} L_{2k+1}\left(ih_{2k+1}a\right)\beta_{2k+1}\cos\left(\dfrac{2k+1}{2}\pi\ u\right) \\ +L_{2k+2}\left(ih_{2k+2}a\right)\beta_{2k+2}\sin\left((k+1)\pi\ u\right)\end{array}\right\} = \\ &-i2A\kappa_1\sin\theta_t e^{ik_1 y_t\sin\theta_t}e^{-ik_0\cos\theta_0 x} \\ &-\sum_{m=0}^{\infty}\int_0^{\infty}\frac{\sqrt{\xi^2-\kappa_1^2}}{\xi}\left\{ F_m G_{2m+1}^C(\xi) + G_m G_{2m+2}^S(\xi)\right\} d\xi \\ &+\sum_{m=0}^{\infty}\int_0^{\infty}\frac{\sqrt{\xi^2-\kappa_1^2}}{\xi}\left\{ H_m G_{2m+1}^C(\xi) + K_m G_{2m+2}^S(\xi)\right\} e^{-t\sqrt{\xi^2-\kappa_1^2}}d\xi , \end{aligned} \tag{17}$$

where $\gamma(.) = \left\{1 - e^{ih(.)2b}\right\}$, $\beta(.) = \left\{1 + e^{ih(.)2b}\right\}$, Gc and Gs are

$$\begin{cases} G_\tau^C(\xi) = J_\tau(\xi)\cos(\xi u) \\ G_\tau^S(\xi) = J_\tau(\xi)\sin(\xi u) \ . \end{cases} \tag{18}$$

These equations are solved by KP method and separated into odd and even groups in accordance with Euler's formula. One may end up with the following simultaneous equations.

$BC.1$: *Even Identity*:

$$\sum_{m=0}^{\infty}D_m\int_0^{\infty}P(\xi)e^{-t\sqrt{\xi^2-\kappa_0^2}}d\xi = \sum_{m=0}^{\infty}F_m\int_0^{\infty}P(\xi)e^{-t\sqrt{\xi^2-\kappa_1^2}}d\xi + \sum_{m=0}^{\infty}H_m\int_0^{\infty}P(\xi)d\xi. \tag{19}$$

$BC.1$: *Odd Identity*:

$$\sum_{m=0}^{\infty}E_m\int_0^{\infty}Q(\xi)e^{-t\sqrt{\xi^2-\kappa_0^2}}d\xi = \sum_{m=0}^{\infty}G_m\int_0^{\infty}Q(\xi)e^{-t\sqrt{\xi^2-\kappa_1^2}}d\xi + \sum_{m=0}^{\infty}K_m\int_0^{\infty}Q(\xi)d\xi. \tag{20}$$

$BC.2$: *Even Identity*:

$$\begin{aligned} &\mu_1\sum_{m=0}^{\infty}D_m\int_0^{\infty}\sqrt{\xi^2-\kappa_0^2}P(\xi)e^{-t\sqrt{\xi^2-\kappa_0^2}}d\xi = \\ &\sum_{m=0}^{\infty}F_m\int_0^{\infty}\sqrt{\xi^2-\kappa_1^2}P(\xi)e^{-t\sqrt{\xi^2-\kappa_1^2}}d\xi - \sum_{m=0}^{\infty}H_m\int_0^{\infty}\sqrt{\xi^2-\kappa_1^2}P(\xi)d\xi. \end{aligned} \tag{21}$$

$BC.2$: *Odd Identity*:

$$\begin{aligned} &\mu_1\sum_{m=0}^{\infty}E_m\int_0^{\infty}\sqrt{\xi^2-\kappa_0^2}Q(\xi)e^{-t\sqrt{\xi^2-\kappa_0^2}}d\xi = \\ &\sum_{m=0}^{\infty}G_m\int_0^{\infty}\sqrt{\xi^2-\kappa_1^2}Q(\xi)e^{-t\sqrt{\xi^2-\kappa_1^2}}d\xi - \sum_{m=0}^{\infty}K_m\int_0^{\infty}\sqrt{\xi^2-\kappa_1^2}Q(\xi)d\xi. \end{aligned} \tag{22}$$

$BC.3$: *Even Identity*:

$$(-1)^k\left\{L_{2k+1}\gamma_{2k+1}\right\} = \frac{2}{2k+1}\sum_{m=0}^{\infty}J_{2m+1}\left((2k+1)\frac{\pi}{2}\right)\left\{\begin{array}{l} F_m \\ e^{-t\sqrt{\left((2k+1)\frac{\pi}{2}\right)^2-\kappa_1^2}}H_m \end{array}\right\}. \tag{23}$$

$$BC.3: Odd\ Identity:$$

$$(-1)^k \left\{ L_{2k+2}\gamma_{2k+2} \right\} = \frac{1}{k+1}\sum_{m=0}^{\infty} J_{2m+2}((k+1)\pi) \begin{Bmatrix} G_m \\ e^{-t\sqrt{((k+1)\pi)^2-\kappa_1^2}} K_m \end{Bmatrix}. \tag{24}$$

$$BC.4: Even\ Identity:$$

$$\frac{\mu_1}{\mu_r}\sum_{k=0}^{\infty}(-1)^k \left\{ L_{2k+1}\beta_{2k+1}(ih_{2k+1}a)\frac{J_{2n+1}\left((2k+1)\frac{\pi}{2}\right)}{(2k+1)\frac{\pi}{2}} \right\} =$$
$$i2Ak_1 \sin\theta_t e^{ik_1 y_t \sin\theta_t} \frac{J_{2n+1}(\kappa_0 \cos\theta_0)}{\kappa_0 \cos\theta_0}$$
$$+\sum_{m=0}^{\infty} F_m \int_0^{\infty} \sqrt{\xi^2-\kappa_1^2}\,P(\xi)d\xi - \sum_{m=0}^{\infty} H_m \int_0^{\infty} \sqrt{\xi^2-\kappa_1^2}\,P(\xi)e^{-t\sqrt{\xi^2-\kappa_1^2}}d\xi. \tag{25}$$

$$BC.4: Odd\ Identity:$$

$$\frac{\mu_1}{\mu_r}\sum_{k=0}^{\infty}(-1)^k \left\{ L_{2k+2}\beta_{2k+2}(ih_{2k+2}a)\frac{J_{2n+2}((k+1)\pi)}{(k+1)\pi} \right\} =$$
$$2Ak_1 \sin\theta_t e^{ik_1 y_t \sin\theta_t} \frac{J_{2n+2}(\kappa_0 \cos\theta_0)}{\kappa_0 \cos\theta_0}$$
$$+\sum_{m=0}^{\infty} G_m \int_0^{\infty} \sqrt{\xi^2-\kappa_1^2}\,Q(\xi)d\xi - \sum_{m=0}^{\infty} K_m \int_0^{\infty} \sqrt{\xi^2-\kappa_1^2}\,Q(\xi)e^{-t\sqrt{\xi^2-\kappa_1^2}}d\xi. \tag{26}$$

where

$$P(\xi) = \frac{J_{2m+1}(\xi)J_{2n+1}(\xi)}{\xi^2}$$
$$Q(\xi) = \frac{J_{2m+2}(\xi)J_{2n+2}(\xi)}{\xi^2}. \tag{27}$$

Equations (19) to (26) are eight sets of equations to be solved for eight sets of unknown coefficients D_m, E_m, F_m, G_m, H_m, K_m, L_{2k}, L_{2k+1}. In a cylindrical coordinate system where the observation point is represented by ρ and θ the far-field scattering is [29],

$$\phi_1^s = \sqrt{\frac{\pi}{2k_0\rho}}\, e^{i_1\left(k_0\rho + \pi/4\right)} \sum_{m=0}^{\infty} \begin{Bmatrix} D_m J_{2m+1}(k_0 a\cos\theta) \\ -iE_m J_{2m+2}(k_0 a\cos\theta) \end{Bmatrix}. \tag{28}$$

The above summations are all convergent and therefore, n and m are limited to N and M, respectively.

III. VALIDATION AND NUMERICAL RESULTS

In this section different simulations for both filled and coated cracks are given. Two approaches are utilized for validation of this method. First, FEM calculates the equivalent magnetic current density $|M_x|$ on the aperture for several incident angles. Second, for rigorous validation, convergence analysis is performed by changing the truncation numbers N and M [33]. Different cases of the simulations are listed in Table 1.

A. Magnetic current density analysis

Referring to Fig. 1 and Table 1, in the case (a), the non-filled crack is coated by a dielectric layer with a complex permittivity and permeability, while in the case (b); the crack is additionally filled by a complex material. Figure 2 shows the equivalent magnetic current density distribution, $|M_x|$ on the crack ($|x| < a$, $y = 0$) for various incident angles (θ_0 = 15°, 30°, 45°, 60°, 75°, 90°). In this figure, truncation number of the series is assumed to be N, M = 14. Comparison of the results with the FEM solution demonstrates the accuracy of the method for all incident angles. We plot the electric field distribution, calculated by KP method, at normal incident angle for case (b) (see Fig. 3). As shown, the boundary conditions are satisfied at the edges of the crack ($x / \lambda_0 = \pm 1$, $y / \lambda_0 = 0$), while the field maximum occurs near the slab layer ($y / \lambda_0 = 1$). It can also be observed that the field values at $y / \lambda_0 = 1$ is equal to the black solid line in Fig. 2 where $\theta_0 = 90°$.

Table 1: Different scenarios of coated/filled cracks.

	$2a$	b	ε_r	μ_r	ε_1	μ_1	y_t
a	$2\lambda_0$	$1\lambda_0$	1	1	$2 + 0.1i$	$1.4 + 0.1i$	$\lambda_0/10$
b	$2\lambda_0$	$1\lambda_0$	$2.5 + 0.2i$	$1.8 + 0.1i$	$2 + 0.1i$	$1.4 + 0.1i$	$\lambda_0/10$
c	$0.5\lambda_0$	$0.2\lambda_0$	$3 + 0.1i$	$1.2 + 0.02i$	$2.1 + 1.53i$	$1.4 + 0.1i$	$\lambda_0/6$
d	$0.8\lambda_0$	$0.3\lambda_0$	$2.7 + 0.03i$	$1.8 + 0.1i$	$5.33 + 1.53i$	$1.4 + 0.1i$	$\lambda_0/7$
e	$0.9\lambda_0$	$0.5\lambda_0$	$8.42 + 1.03i$	$1.6 + 0.1i$	$3.48 + 0.12i$	$1.2 + 0.2i$	$\lambda_0/5$
f	$2\lambda_0$ [26]	$1\lambda_0$	$2.5 + 0.2i$	$1.8 + 0.1i$	1	1	---
g	$2\lambda_0$ [26]	$1\lambda_0$	1	1	1	1	---
h	$1.5\lambda_0$	$10\lambda_0$	$3.48 + 0.12i$	$1.2 + 0.02i$	1	1	---

B. Convergence analysis

For rigorous validation, the error analysis is carried out and the convergence curves are represented in Fig. 4 for various cases c, d, and e. The error function and Euclidean norm are

$$\begin{cases} e_r = \left\| M_{x_k}^{i+1} - M_{x_k}^{i} \right\| / \left\| M_{x_k}^{i} \right\|, \quad i = 1..N, \\ \left\| M_{x_k}^{i} \right\| = \sqrt{\sum_{k=1}^{K} \left| M_{x_k}^{i} \right|^2} \end{cases} \tag{29}$$

where x_k denotes the position of the k^{th} point on the crack and K represents the total number of the observation points. The results are calculated using $K = 25$ for all three cases.

According to Fig. 4, the summations converge rapidly, such that for N and M close to 8~10, the error is equal to $10^{-1.7} = 0.02$. This result is expectable due to the fact that Weber-Schafheitlin type integrals satisfy the boundary condition on the PEC ($|x| > a$, $v = 0$) automatically. The rapid convergence of the analytic method makes it desirable for efficient calculation of the scattered field in the inverse problems.

C. Results

In this section, we compute backscattered RCS, bistatic RCS, and far-field scattering patterns for several filled and coated cracks. We make comparisons with other computed results of the backscattered RCS for the simpler geometry, such as the case of no coating layer. Figure 5 shows the normalized backscattered RCS of cases f and g from Table 1 and compare the results of this method with those on [26]. A very good agreement is observed between these methods. Cases of coated layer with height $y_t = \lambda_0 / 3$ and relative permittivity $\varepsilon_1 = 3 + 0.1i$ and relative permeability $\mu_1 = 1.6 + 0.2i$ are also simulated. Black dash line and cyan dot line depict the results of proposed method for coated cases f and g, respectively. Observation shows that coating layer on the crack alters the RCS signature significantly.

Figure 6 shows the variation of the normalized RCS versus observation angle for case g where the crack is coated by various materials. The crack is illuminated by an incident plane wave at $\theta_0 = 45^{\circ}$. Additionally, the depth of the dielectric layer is assumed $y_t = 0.6\,\lambda_0$ for all of the coating layers. As shown the dielectric constant of the layer does not have a monotonic effect on RCS. Additionally, RCS drops down when very lossy material coats the crack (solid pink line with diamonds).

Next, to show the validity of the proposed method for narrow cracks the normalized backscattering RCS of the case g is presented in Fig. 7. We also coat this case by a material with $\varepsilon_1 = 2.7 + 0.03i$, $\mu_1 = 1.4 + 0.1i$ and the thickness of $y_t = \lambda_0/4$.

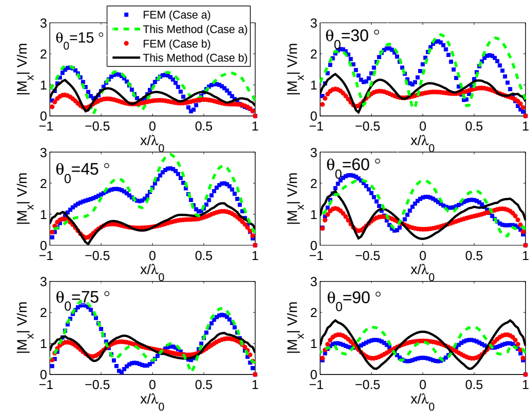

Fig. 2. Magnetic current densities on the crack ($|x| < a$, $y = 0$) computed by the proposed method and FEM for cases a and b.

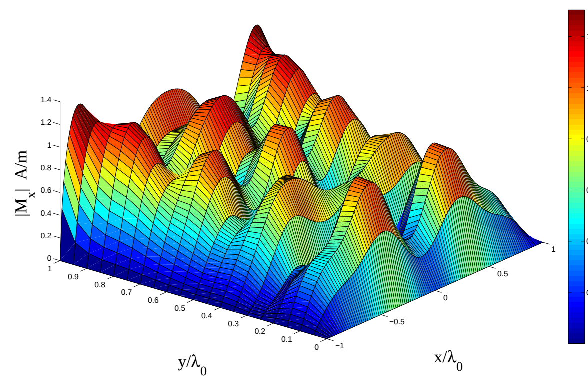

Fig. 3. Distribution of magnetic current density in the crack computed by the KP method for crack of case b.

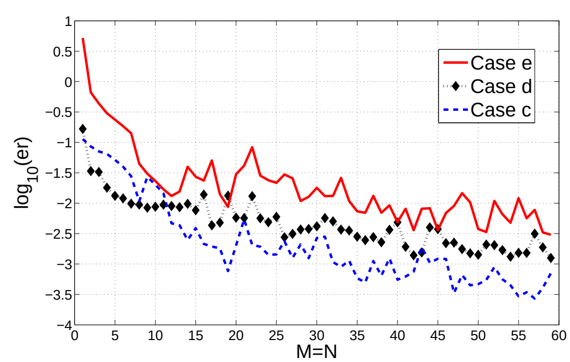

Fig. 4. Convergence curves for cases c, d, and e.

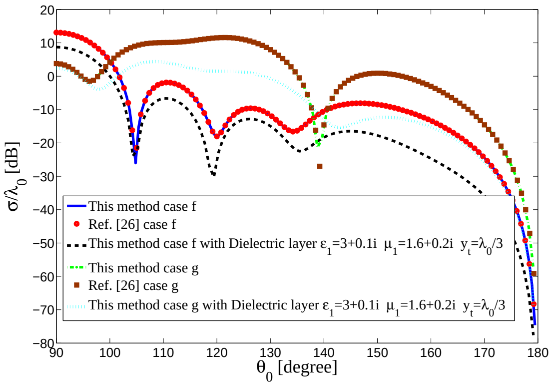

Fig. 5. Normalized RCS as a function of incident angles for case e, and with a dielectric layer of case f.

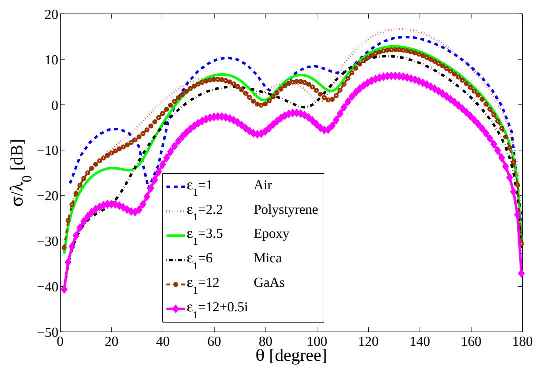

Fig. 6. Normalized bistatic RCS of the crack versus observation angle for various coated dielectric materials of case g.

The variation of the normalized RCS versus the dielectric layer thickness for various permittivity and permeability are shown in Figs. 8 and 9, respectively. The parameters of the crack are w = 0.2 λ_0 and b = 0.2 λ_0, also it is illuminated by normal plane wave. In addition, the cracks in all cases are filled by rust with $\varepsilon_r = 2.7 + 0.03i$ and μ_r = 1. As shown in Fig. 8 when the dielectric constant increases, normalized RCS almost increases. According to Figs. 8 and 9, by increasing the dielectric slab thickness RCS has oscillatory behaviour.

Next, the scattering far-field pattern for an empty and covered crack with $w = b$ and $2ka = 15$ is shown in Fig. 10. We compare our results with those on [26] for non-coated crack. The crack is coated by a common paint with relative dielectric constant $\varepsilon_1 = 3 + 0.1i$ and height of $y_t = 0.6\ \lambda_0$ for plane-wave incident angle of $\theta_0 = 30^{\circ}$. Also, the crack is coated by a layer of salt rust with relative dielectric of $\varepsilon_1 = 5.33 + 1.53i$ height of $y_t = 0.5\ \lambda_0$ for plane-wave incident angle of $\theta_0 = 75^{\circ}$.

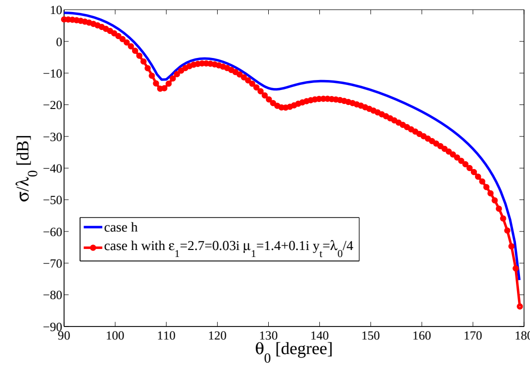

Fig. 7. Normalized backscattering RCS of the narrow crack of case h and this case with a λ_0 / 4 dielectric layer of $\varepsilon_1 = 2.7 + 0.03i$ and $\mu_1 = 1.4 + 0.1i$.

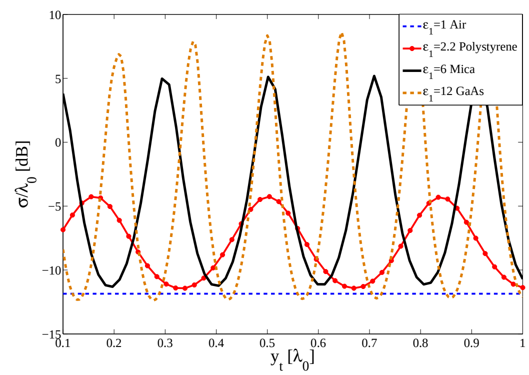

Fig. 8. Normalized RCS of the crack with w = $0.2\lambda_0$, $b = 0.2\lambda_0$ as a function of coating thickness for different permittivities.

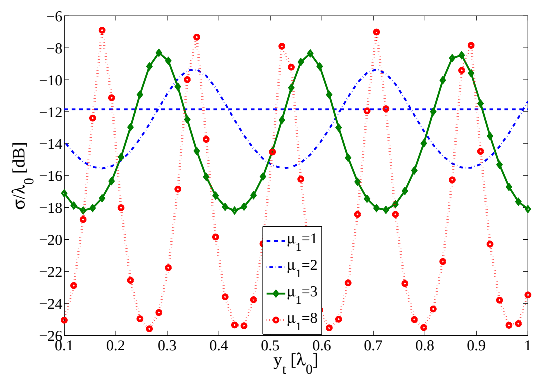

Fig. 9. Normalized RCS of the crack with w = $0.2\lambda_0$, $b = 0.2\lambda_0$, $\varepsilon_r = 2.7 + 0.03i$, $\mu_r = 1$ versus paint thickness for different permeabilities.

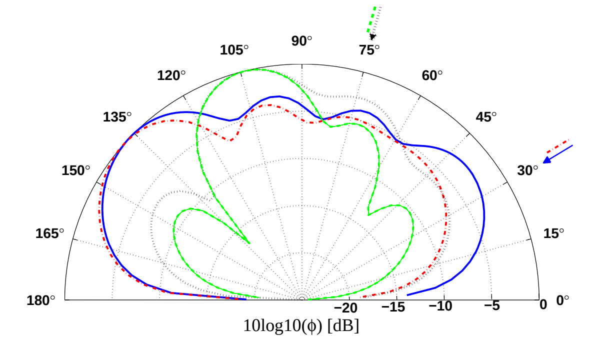

Fig. 10. Scattering far-field pattern for an empty crack where $w = b$ and $2ka = 15$.

——: $(\theta_0 = 30^\circ, \varepsilon_1 = 1, \mu_1 = 1)$, Ref.[26],

— · —: $(\theta_0 = 30^\circ, \varepsilon_1 = 3 + 0.1i, \mu_1 = 1, y_t = 0.6\lambda_0)$,

.......: $(\theta_0 = 75^\circ, \varepsilon_1 = 1, \mu_1 = 1)$, Ref.[26],

— —: $(\theta_0 = 75^\circ, \ \varepsilon_1 = 5.33 + 1.53i, \mu_1 = 1, y_t = 0.5\lambda_0)$.

As shown a thin layer of lossy dielectric alters the scattering pattern significantly. The maximum scattering peak value occurs at the vicinity of the corresponding specular direction for both cases of incident angles. Finally, in Fig. 11, the scattering far-field pattern for a crack with $w = b$ and $2ka = 5$ is shown. We compare our results with those on [26] for non-coated crack. Relative permittivity and relative permeability of $\varepsilon_r = 2.5 + 0.2i$ and $\mu_r = 1.8 + 0.1i$ are used to fill the crack and Fe_2O_3 powder (Rust) with relative dielectric constant $\varepsilon_1 = 2.7 + 0.03i$ and height of $y_t = 0.7\ \lambda_0$ is utilized to cover the crack. Additionally, the results are shown for two incident angles $\theta_0 = 15^\circ, 60^\circ$. As shown in Fig. 11, scattering pattern varies significantly even for a thin layer of coating layer.

IV. CONCLUSION

In this paper, we analyzed the EM plane wave scattering of a 2D rectangular filled and coated crack on a ground plane by the use of KP method for the TM case. The validation of the proposed method was accomplished by utilizing two techniques; consisting of FEM to investigate the equivalent magnetic current density on the aperture and the convergence analysis. The proposed method is shown to be accurate for both narrow and wide cracks and also is applicable to all lossy and lossless materials for filled and coated cracks. In addition, the sensitivity of RCS to permittivity, permeability, and thickness of the overlaying layer was presented.

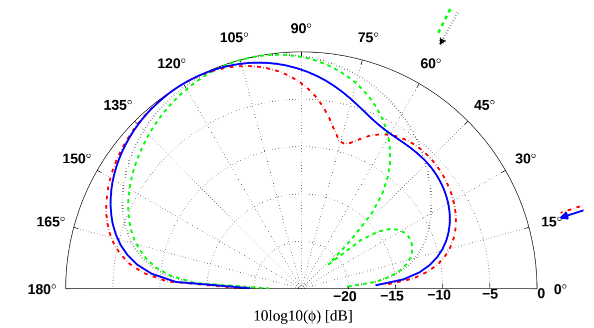

Fig. 11. Scattering far-field pattern for a crack where $w = b$, $2ka = 5$, $y_t = \lambda_0 / 7$, and dielectric filled material characteristics are depicted in the figure legend

——: $(\theta_0 = 15^\circ, \varepsilon_1 = 1, \mu_1 = 1)$, non-filled, Ref.[26],

— · —: $(\theta_0 = 15^\circ, \varepsilon_1 = 2.7 + 0.03i, \mu_1 = 1, y_t = 0.7\lambda_0)$, filled,

.......: $(\theta_0 = 60^\circ, \varepsilon_1 = 1, \mu_1 = 1)$, non-filled, Ref.[26],

— —: $(\theta_0 = 60^\circ, \ \varepsilon_1 = 2.7 + 0.03i, \mu_1 = 1, y_t = 0.7\lambda_0)$, filled.

ACKNOWLEDGMENT

The authors would like to thank Iran Telecommunication Research Center (ITRC) for supporting this work. The authors also wish to express their gratitude to Prof. Q. A. Naqvi at Quad-i-Azam University for his valuable inputs.

APPENDIX
STANDING WAVES IN THE SLAB

A dielectric slab on an infinite PEC ground is shown in Fig. A. The height of the slab is y_t and the relative permittivity and relative permeability of $\varepsilon_1$and μ_1, respectively are the material characterization of the slab. Here, $k_0 = \omega\sqrt{\varepsilon_0\mu_0}$ and $k_1 = k_0\sqrt{\varepsilon_1\mu_1}$ are respectively the free space and the dielectric slab wave numbers. The slab is illuminated by a TM polarized EM plane wave,

$$\phi^i\left(= E_z^i\right) = e^{-ik_0(x\cos\theta_0 + y\sin\theta_0)}, \tag{A.1}$$

and the reflected plane wave is,

$$\phi^r\left(= E_z^r\right) = \mathrm{R}e^{-ik_0(x\cos\theta_0 - y\sin\theta_0)}, \tag{A.2}$$

where, R is the reflection coefficient, θ_0 is the incident angle, θ_t is the transmission angle. Assuming ψ is the total electric field in the dielectric slab. Therefore,

$$\psi = \left[A e^{-ik_1 \sin\theta_t (y - y_t)} + B e^{+ik_1 \sin\theta_t y} \right] e^{-ik_1 \cos\theta_t x}, \qquad \text{(A.3)}$$

where A and B are unknown coefficients. The first term and the second term in (A.3) describe the down-going and the up-going wave, respectively. In order to find the aforementioned unknowns first, we note that the tangential electric field is zero over the PEC boundary ($y = 0$), thus,

$$B = -A e^{ik_1 y_t \sin\theta_t}, \qquad \text{(A.4)}$$

Second, imposing the continuity of the tangential field components E_z and H_x at $y = y_t$ yields,

$$A = \frac{2e^{-ik_0 y_t (\sin\theta_0)}}{1 + \dfrac{k_1 \sin\theta_t}{\mu_1 k_0 \sin\theta_0} + e^{ik_1 2 y_t (\sin\theta_t)} \left[-1 + \dfrac{k_1 \sin\theta_t}{\mu_1 k_0 \sin\theta_0} \right]}, \qquad \text{(A.5)}$$

and

$$R = \frac{\dfrac{k_1 \sin\theta_t}{\mu_1 k_0 \sin\theta_0} \left[1 + e^{ik_1 2 y_t (\sin\theta_t)} \right] - 1 + e^{ik_1 2 y_t (\sin\theta_t)}}{-\dfrac{k_1 \sin\theta_t}{\mu_1 k_0 \sin\theta_0} \left[1 + e^{ik_1 2 y_t (\sin\theta_t)} \right] - 1 + e^{ik_1 2 y_t (\sin\theta_t)}} \qquad \text{(A.6)}$$

$$.e^{-ik_0 2 y_t (\sin\theta_0)}.$$

Thus, the electric field in dielectric slab can be expressed as,

$$\psi = A \left[e^{-ik_1 (y - y_t) \sin\theta_t} - e^{+ik_1 (y + y_t) \sin\theta_t} \right] e^{-ik_1 \cos\theta_t x}. \qquad \text{(A.7)}$$

where A is given in equation (A.5).

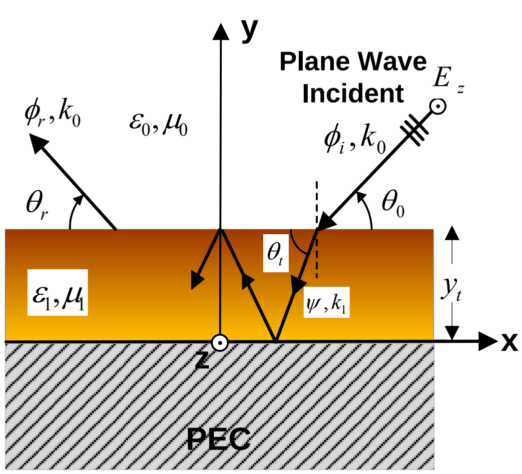

Fig. A. Geometry of a dielectric slab on an infinite ground plane.

REFERENCES

[1] M. T. Ghasr, S. Kharkovsky, and R. Zoughi, “Comparison of near-field millimeter-wave probes for detecting corrosion precursor pitting under paint,” *IEEE Trans. on Instrumentation and Measurement*, vol. 54, no. 4, pp. 1497-1504, August 2005.

[2] A. McClanahan, S. Kharkovsky, A. R. Maxon, R. Zoughi, and D. D. Palmer, “Depth evaluation of shallow surface cracks in metals using rectangular waveguides at millimeter-wave frequencies,” *IEEE Trans. on Instrumentation and Measurement*, vol. 59, no. 6, pp. 1693-1704, June 2010.

[3] N. Qaddoumi, A. Shroyer, and R. Zoughi, “Microwave detection of rust under paint and composite laminates,” *Taylor and Francis Journal: Research in Nondestructive Evaluation*, vol. 9, no. 4, pp. 201-212, June 1997.

[4] A. M. Albishi, M. S. Boybay, and O. M. Ramahi, “Complementary split-ring resonator for crack detection in metallic surfaces,” *IEEE Microw. Wireless Compon. Lett.*, vol. 22, no. 6, pp. 330-332, June 2012.

[5] J. Kerouedan, P. Queffelec, P. Talbot, C. Quendo, and A. L. Brun, “Detecting of micro-cracks on metal surfaces using near field microwave dual behaviour resonators,” *Springer, New Developments and App. in Sen. Tech*, vol. 83, pp. 1-13, 2011.

[6] S. Kharkovsky, A. McClanahan, R. Zoughi, and D. D. Palmer, “Microwave dielectric-loaded rectangular waveguide resonator for depth evaluation of shallow flaws in metals,” *IEEE Trans. on Instrumentation and Measurement*, vol. 60, no. 12, pp. 3923-3930, Dec. 2011.

[7] W. D. Wood and A. W. Wood, “Development and numerical solution of integral equations for electromagnetic scattering from a trough in a ground plane,” *IEEE Trans. Antennas Propagat.*, vol. 47, no. 8, pp. 1318-1322, August 1999.

[8] T. B. A. Senior, K. Sarabandi, and J. R. Natzke, “Scattering by a narrow gap,” *IEEE Trans. Antennas Propagat.*, vol. 38, no. 7, pp. 1102-1111, July 1990.

[9] T. B. A. Senior and J. L.Volakis, “Scattering by gaps and cracks,” *IEEE Trans. Antennas Propagat.*, vol. 37, no. 6, pp. 744-750, June 1989.

[10] K. Barkeshli and J. L. Volakis, “TE scattering by a two-dimensional groove in a ground plane using higher order boundary conditions,” *IEEE Trans. Antennas Propagat.*, vol. 38, no. 9, pp. 1421-1428, Sep. 1990.

[11] K. Barkeshli and J. L. Volakis, “Scattering from narrow rectangular filled grooves,” *IEEE Trans. Antennas Propagat.*, vol. 39, no. 6, pp. 804-810, June 1991.

[12] T. J. Park, H. J. Eom, and K. Yoshitomi, "An analytic solution for transverse-magnetic scattering from a rectangular channel in a conducting plane," *Journal of Appl. Phys.*, vol. 73, no. 7, pp. 3571-3573, April 1993.

[13] J. Jin, *The Finite Element Method in Electromagnetics*: John Wiley & Sons, 2002.

[14] K. Du, "Two transparent boundary conditions for the electromagnetic scattering from two-dimensional overfilled cavities," *Elsevier Journal of Computational Physics* pp. 5822-5835 2011.

[15] Y. H. Cho, "TM scattering from finite rectangular grooves in a conducting plane using overlapping T-block analysis," *IEEE/ACES Conf. on Wireless Commun. and Appl. Comp. Electro., Society (ACES)*, pp. 744-747, 2005.

[16] Y. H. Cho, "TM plane-wave scattering from finite rectangular grooves in a conducting plane using overlapping T-block method," *IEEE Trans. Antennas Propagat.*, vol. 54, no. 2, pp. 746-749, Feb. 2006.

[17] Y. H. Cho, "Transverse magnetic plane-wave scattering equations for infinite and semi-infinite rectangular grooves in a conducting plane," *IET Microwaves, Antennas & Propagation*, vol. 2, no. 7, pp. 704-710, March 2008.

[18] M. A. Morgan and F. K. Schwering, "Mode expansion solution for scattering by a material filled rectangular groove," *Progress in Electromagnetics Research (PIER)*, vol. 18, pp. 1-17, 1998.

[19] G. Bao, J. Gao, J. Lin, and W. Zhang, "Mode matching for the electromagnetic scattering from three-dimensional large cavities," *IEEE Trans. Antennas Propag.*, vol. 60, no. 4, pp. 2004-2010, April 2012.

[20] F. Deek and M. El-Shenawee, "Microwave detection of cracks in buried pipes using the complex frequency technique," *Appl. Comp. Electro. Society (ACES) Journal*, vol. 25, no. 10, pp. 894-902 2010.

[21] M. Bozorgi and A. Tavakoli, "Backscattering from a two dimensional rectangular crack using FIE," *IEEE Trans. Antennas Propag.*, vol. 58, no. 2, pp. 552-564, Feb. 2010.

[22] M. Bozorgi and A. Tavakoli, "Polarimetric scattering from a 3-D rectangular crack in a PEC covered by a dielectric layer," *Appl. Comp. Electro. Society (ACES) Journal*, vol. 26, no. 6, pp. 502-510, June 2011.

[23] B. Honarbakhsh and A. Tavakoli, "Scattering by a 2D crack: The mesh free collocation approach," *Appl. Comp. Electro. Society (ACES) Journal*, vol. 27, no. 3, pp. 278-284, March 2012.

[24] K. Hongo, A. D. U. Jafri, and Q. A. Naqvi, "Scattering of electromagnetic spherical wave by a perfect conducting disk," *Progress In Electromagnetics Research (PIER)*, vol. 129, pp. 315-343, 2012.

[25] A. Imran, Q. A. Naqvi, and K. Hongo, "Diffraction of electromagnetic plane wave from a PEMC strip," *International Journal of Applied Electromagnetics and Mechanics*, vol. 34, no. 3, pp. 181-193, Jan. 2010.

[26] R. Sato and H. Shirai, "Electromagnetic wave scattering by a trough on a ground --E polarization case--," *Memoirs of The Faculty of Education, Niigata University*, vol. 39, no. 1, pp. 1-9, Sep. 1997.

[27] R. Sato and H. Shirai, "Electromagnetic wave scattering by two rectangular troughs on a ground plane," *IEEE AP-S International Symposium and USNC/URSI National Radio Science URSI Meeting*, Utah USA, 2000.

[28] R. Sato and H. Shirai, "EM scattering analysis by a loaded trough on a ground plane using SIBC-E polarization case," *IEEE Antennas and Propagation Society Int. Symp. Digest*, 1999.

[29] H. Shirai and H. Sekiguchi, "A simple crack depth estimation method from backscattering response," *IEEE Trans. on Instrumentation and Measurement*, vol. 53, no. 4, pp. 1249-1254, Aug. 2004.

[30] R. Sato and H. Shirai, "Propagation analysis for a simplified indoor/outdoor interface model," *IEEE Antennas and Propagation Society Int. Symp. Digest, AP-S*. Nigata, Japan, 2010.

[31] K. Hongo and Q. A. Naqvi, "Similarities between moment method and Kobayashi potential," *IEICE General Conference*, Kusatsu, Japan, 2001.

[32] B. Ghalamkari, M. Dehmollian, and A. Tavakoli, "Analytical solution of scattering by a 2D dielectric filled crack in a ground plane coated by a dielectric layer: TE case," *To Be Published in Appl. Comp. Electro. Society (ACES) Journal*.

[33] J. C. Rautio, "The microwave point of view on software validation," *IEEE Antennas Propagat. Mag.*, vol. 38, no. 2, pp. 68-71, April 1996.

Behbod Ghalamkari was born in Tehran, Iran, on December 5, 1981. He received B.Sc. degree in Electrical Engineering from Semnan University of Semnan, Semnan, Iran, in 2005, the M.Sc. degree from the Amirkabir University of Technology (Tehran Polytechnic), Tehran, Iran, in 2007, both in Electrical Engineering. He is currently working toward the Ph.D. degree in Electrical Engineering in Amirkabir University of Technology. His main interest lies in the electromagnetic wave propagation, scattering and optimization in electromagnetic problems.

Ahad Tavakoli was born in Tehran, Iran, on March 8, 1959. He received the B.Sc. and M.Sc. degrees from the University of Kansas, Lawrence, and the Ph.D. degree from the University of Michigan, Ann Arbor, all in Electrical Engineering, in 1982, 1984, and 1991, respectively.
He is currently a Professor in the Department of Electrical Engineering at Amirkabir University of Technology. His research interests include EMC, scattering of electromagnetic waves and microstrip antennas.

Mojtaba Dehmollaian was born in Iran in 1978. He received the B.Sc. and M.Sc. degrees in Electrical Engineering from the University of Tehran, Tehran, Iran, in 2000 and 2002, respectively. He received the M.Sc. degree in applied mathematics and Ph.D. degree in Electrical Engineering from the University of Michigan, Ann Arbor, in 2007.
Currently, he is an Assistant Professor with the Department of Electrical and Computer Engineering, University of Tehran. His research interests are applied electromagnetics, radar remote sensing, electromagnetic wave propagation, and scattering.